Award Number: G09AP00117

CREEP EVENTS ON THE SOUTHERN SAN ANDREAS FAULT: MODELING AND MEASUREMENT

Start and End Dates: 7/1/2009 to 6/30/2010

Final Technical Report, February 25, 2011

Duncan Carr Agnew

Institute of Geophysics and Planetary Physics
Scripps Institution of Oceanography
University of California, San Diego
La Jolla, CA 92093-0225
(858) 534-2590 (FAX 534-5332); dagnew@ucsd.edu

Award Number: G09AP00117

CREEP EVENTS ON THE SOUTHERN SAN ANDREAS FAULT: MODELING AND MEASUREMENT

Duncan Carr Agnew

Abstract

This grant supported data analysis and modeling of strainmeter data collected in the vicinity of the southernmost section of the San Andreas fault, to better understand the source of aseismic events observed there. We have developed a novel approach to inverting the observed data for possible locations and sizes of events, which is applicable to any number of observations but especially useful when there are few. We also studied aseismic strains that followed the El-Mayor/Cucapah earthquake, which occurred on 2010:094. This appears to have triggered, as well as immediate and rapidly-decaying deformations (most likely caused by afterslip on the rupture zone), but also creep on the San Andreas fault, with events occurring several hours after the mainshock.

Report

1. Introduction

This report covers work done on a program of modeling and measurements to improve our understanding of aseismic strain events that have been observed at the southern end of the southern San Andreas fault, at Durmid Hill, on the laser strainmeters and creepmeters installed there. The largest sequence of such events began in April 2008; anomalous strains in this area are of special interest because the Coachella segment of the San Andreas, on which these events happen, has an 8-m slip deficit, and its southernmost end, where these strain changes are seen, is a possible initiation point for a future great earthquake. We were funded to:

- Model the aseismic strain events seen on the strainmeters at Durmid Hill, using both the strainmeter data and nearby creepmeter data (collected by Prof. Roger Bilham) to constrain the spatial and temporal history of slip.
- Densify long-term measurements of motion around the junction of the southern San Andreas fault and the Brawley Seismic Zone, by re-observing points previously surveyed using GPS. This second activity was not pursued because of redundancy with surveys done by Brendan Crowell, a graduate student at Scripps, under the supervision of Dr. Yehuda Bock.

  We also did not pursue this because of the level of effort given to something not included, for obvious reasons, in our proposal, but still occurring in the period of this grant: analyzing the data collected following the El-Mayor/Cucupah earthquake on April 4, 2010. This was the third-largest shock in southern California in the last 150 years (and probably the largest in the Salton Trough for the last 200); it also was the best recorded in terms of immediate postseismic motions, thanks to the widespread coverage provided by continuous GPS, and longbase and laser strainmeters.

In the first section of this report we describe the history of aseismic strain changes recorded on the southern San Andreas fault from the start of strainmeter measurements in 1994, to late 2010. The section following describes our modeling for some of the largest events; given the sparse data coverage, we have to be satisfied with a less than definite, but still interesting, result. And the third section describes the data and preliminary modeling for the strains observed after the El-Mayor/Cucupah earthquake.

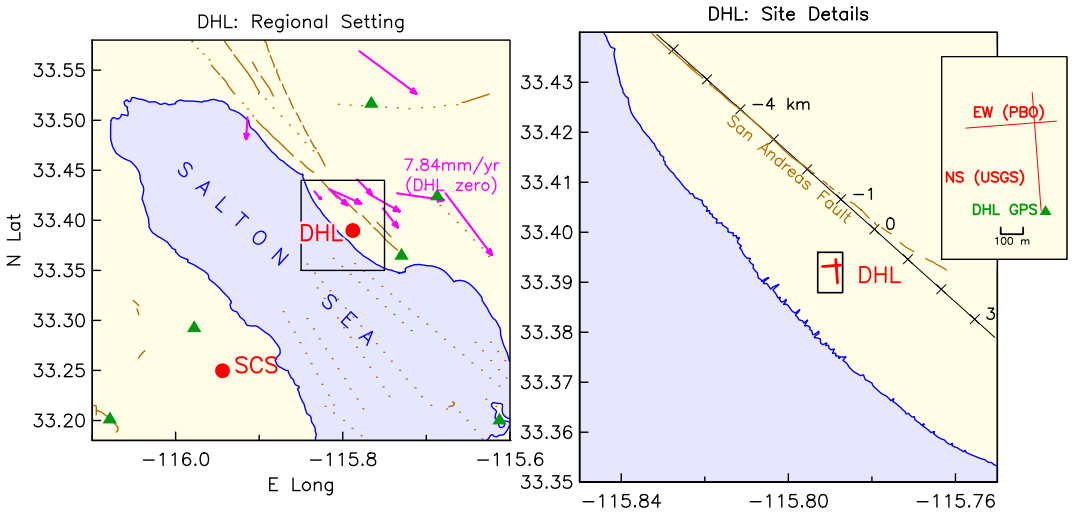

Figure 1

The section of the San Andreas fault zone being considered is, as noted above, ‘‘overdue’’ for a large earthquake, with 8 m of potential slip accumulated since the last large earthquake (or at least slip event) event over 300 years ago; the average recurrence time is about 200 years. The left panel of **Figure 1** shows the location of the strainmeters at DHL: close to the San Andreas fault, and to where it meets the northern extension of the Brawley Seismic Zone. The seismicity of this part of the San Andreas is very low, though the geomorphic expression of the fault is extremely clear. Geodetic measurements show nearly pure shear, with total motion of about 25 mm/yr. DHL is on a large, gentle topographic uplift known as Durmid Hill; the local geology is interbedded claystones and siltstones, much deformed and only weakly cemented together.

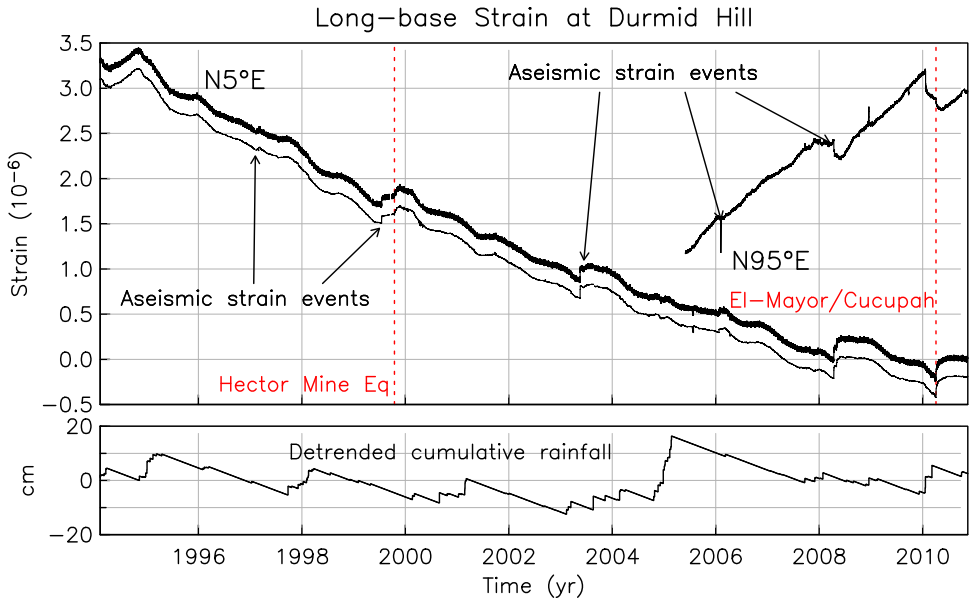

Figure 2

2. Aseismic Strain Events at Durmid Hill

It has been known for some time that on the creeping section of the San Andreas fault between Parkfield and Hollister, much surface slip occurs in brief ‘‘events’’ during which the rate of slip is much higher than at other times; (e.g., Goulty and Gilman 1978, Evans *et al.* 1981; Wesson 1988). At the north end of the creeping section, near San Juan Bautista, several creep events between 1992 and 1998 have been associated with large aseismic strain changes, assumed to be caused by slip on relatively shallow portions of the San Andreas fault (Gladwin *et al.* 1994; Linde *et al.* 1996; Uhrhammer *et al.* 1999).

The southernmost San Andreas is known to have small amounts of ongoing creep (Louie *et al.* 1985, Sieh and Williams 1990, Lyons and Sandwell 2003) and also has experienced creep events triggered by large local earthquakes (Allen *et al.* 1972 [1968 Borrego Mountain earthquake]; Williams *et al.* 1986 [1986 North Palm Springs]; Sharp *et al.* 1989 [1987 Superstition Hills]; Rymer *et al.* 2000 [1992 Landers]; Rymer 2002 [1999 Hector Mine]).

The laser strainmeters at Durmid Hill (DHL) have detected a number of rapid aseismic strain changes which we believe are caused by local creep events. **Figure 2** shows the entire record from both instruments, with these aseismic events labeled; we also plot the rainfall, which has little effect on the NS instrument but can have more on the EW.[1]

Observations with the first of these instruments started in with unanchored operation in early 1994, and with anchoring since late 1994. The first rapid strain change was observed in early 1997, though only on the one instrument then operating. The first unequivocal record of rapid aseismic strain change were in 1999; ‘‘unequivocal’’ because at that time we were operating, with NSF support, a second long-base instrument, installed temporarily to measure earth tides. As these systems shared nothing except the datalogger and line power, we were confident that these events were not instrumental artefacts. Unfortunately there were no creepmeter measurements on the San Andreas fault in this area during the times of these events; a field check for cracking along the fault trace showed no clear evidence of surface fault slip. Buried slip of the amount needed to produce the strain observed would not produce a measurable InSAR signal. These aseismic changes clustered around the time before the 1999 Hector Mine earthquake, ending with a large strain change associated with the shaking from this shock.

We observed an additional slow event in mid-2003 and two more in early 2006, followed by a cluster that produced the largest signal yet, in the spring of 2008. **Figure 3** focuses on the NS instrument from 2006 through 2010 and for context shows local seismicity, creep measured at Ferrum (data provided by Dr. Roger Bilham with NEHRP funding), and motion over a 10-km GPS baseline from DHL across the San Andreas Fault.

These data show several interesting combinations of events and non-events: we see several aseismic strain events. Some of these coincide with creep signals, implying widespread slippage (over at least 10 km of the fault); others do not, and there are also creep events unaccompanied by aseismic strain. These last few years also included a seismic swarm, in early 2009, that caused serious concern about short-term hazard.

We begin with the strain and creep signal seen in early 2008. The creepmeter data (not available earlier) show a clear correlation – though this implies that the slip involved must extend as far south as the strainmeters and as far north as the Ferrum creepmeter, a distance of over 10 km.

Figure 4 shows some of these events, at an expanded scale: comparing **Figure 2** with this figure shows the very wide range, in time and strain, that the longbase instruments can record. So far as we

[1] This is the source of the large offset on that system at the start of 2010; the surrounding drainage has been modified to avoid a repetition.

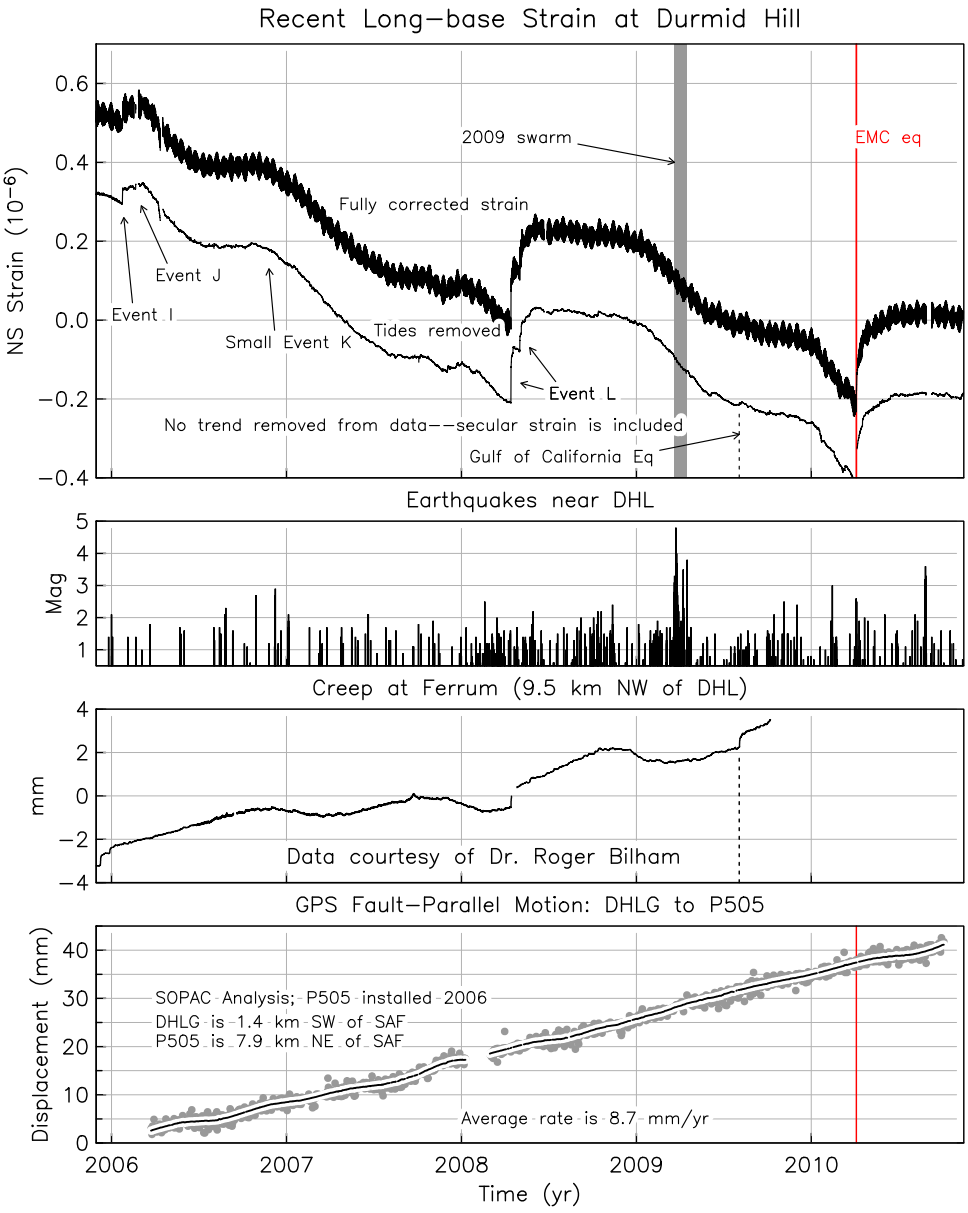

Figure 3

know, these strainmeter records give the highest resolution, both in strain and in time, of any near-field records of aseismic strain changes (compare Goulty and Gilman 1978; King *et al.* 1975; Linde *et al.* 1996; Uhrhammer *et al.* 1999). These detailed records show that individual events are neither similar nor simple, as we discuss in the next section.

The next event of interest was an earthquake swarm in March 2009, which was located in the Salton Sea just south of the transition from the San Andreas fault to the Brawley Seismic zone. **Figure 3** shows the increased level of seismicity. Seismicity in this region is often clustered; since 1980 there have been eight clusters in this region. Clusters before 1990 were relatively small (in terms of maximum magnitude) and were relatively far south of the end of the San Andreas. Since 1999 there have been four clusters, with locations that have, over time, migrated north. The 2009 cluster began with a swarm of activity on March 21, and March 23 there was a magnitude 4.8 event at the northernmost edge of what had been

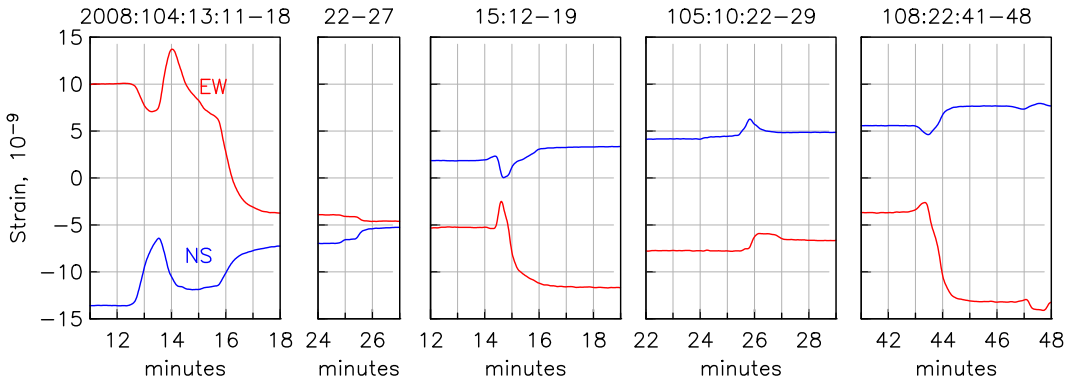

Figure 4

observed previously, which was followed by considerable aftershock activity. The size of the mainshock (the largest in 50 years), and its proximity to the San Andreas, caused concern, since the computations of Agnew and Jones (1991) showed a short-term probability of 5% that this might be a foreshock to a large San Andreas earthquake.

An important source of reassurance during this seismic swarm was that the laser strainmeters at DHL did not show evidence for any unusual deformation. **Figure 5** shows the details of what was observed. The NS instrument optics were thrown out of alignment by the largest event but quickly recentered by remote control. This instrument showed a continuation of steady secular strain accumulation, with no obvious effect from the seismicity. The EW instrument had suffered power problems earlier (for reasons unrelated to the shaking); fixing this accidentally misaligned the optics of one optical anchor, so the data from this instrument was noisy for about three days. However, when this problem was fixed, the secular rate returned to its previous level.

Another 'null' result from the DHL instruments came in July 2009 (day 215) with a magnitude 6.9 earthquake in the Gulf of California (610 km away). The size, proximity, and radiation pattern of this event produced dynamic strains of about $\pm 10^{-6}$ peak to peak. Strains this large from teleseisms are relatively rare, with only three other examples in the last five years (2005:166, magnitude 7.2, 1190 km away; 2004:356, 9.3 and 15000 km away; and 2002:307, 7.8 and 4000 km). For the 2009 data, These large dynamic strains are associated with an immediate step of about 0.2 mm on the Ferrum creepmeter, followed by another 0.2 mm of motion over the next 24 hours, and even more over the next few days (**Figure 3**). The EW long-base strainmeter at DHL showed no offset at a level of 1 nanostrain; the NS instrument did show a change of about 4 nanostrain, though there is some uncertainty about the optical anchoring during this time. Neither strainmeter showed a signal comparable to the slower change on the creepmeter. We thus conclude that the signal seen by the creepmeter does not reflect triggered slip at any depth: it may be something that occurs only in materials very near the surface, though it is surprising that this could be caused by strains of only 10^{-6} in the absence of shaking.

3. Modeling of Creep-Event Data

We have developed models for slip to fit the data described above. The first step of such an inversion is to find the Green function for observed strains or displacements, given slip at a point on the fault plane. For the i-th observable, we write this as $\mathbf{G}_i(x_1, x_2) = \mathbf{G}_i(\mathbf{x})$, where x_1 and x_2 are the horizontal and vertical coordinates along the fault plane, and $\mathbf{x}$ is the corresponding vector. $\mathbf{G}_i$ itself is a vector; the amount of strain or displacement ε produced as a function of time by slip $\mathbf{s}$ on the fault plane (also vector-

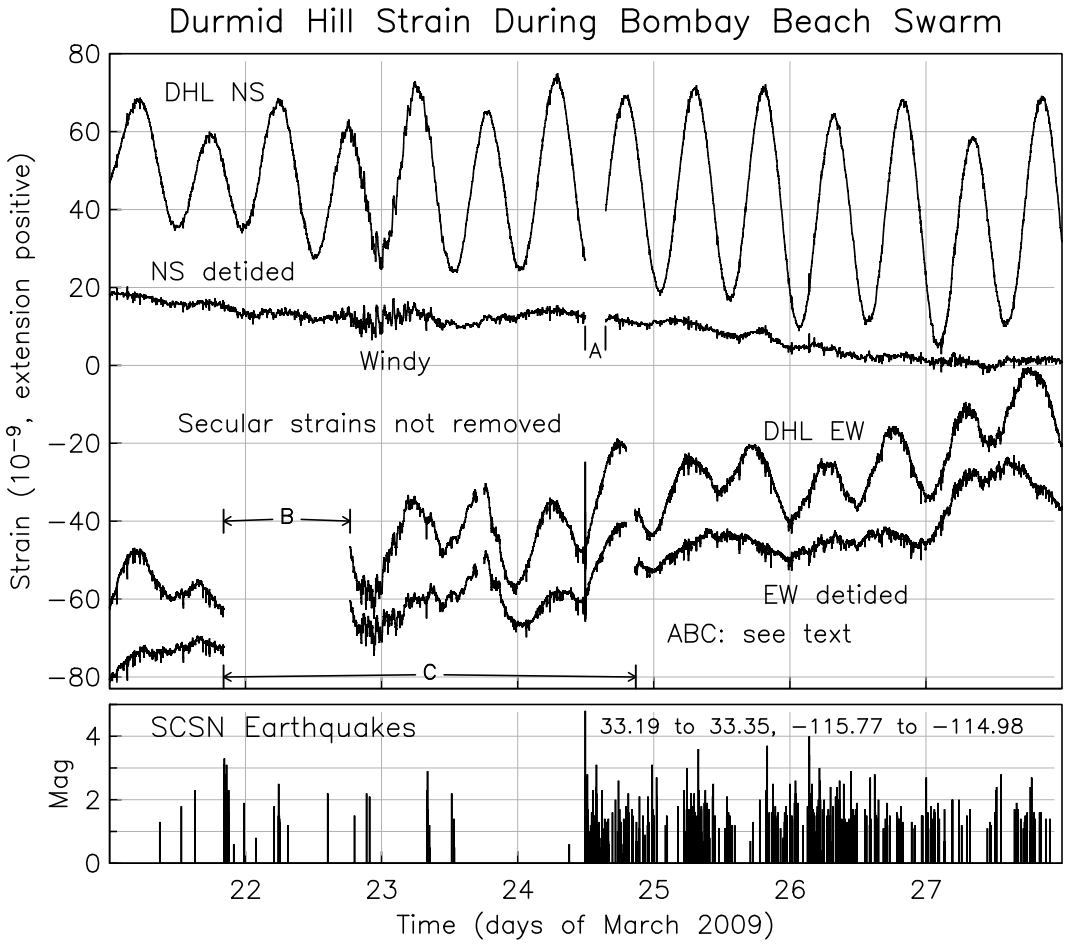

Figure 5

valued) is given by a surface integral over the fault plane P

$$\varepsilon_i(t) = \int_P \mathbf{G}_i(\mathbf{x}) \cdot \mathbf{s}(\mathbf{x}, t)\, dA \tag{1}$$

Since the individual components of $\mathbf{G}_i$ take on a wide range of values, both positive and negative, over the fault surface P, determining $\mathbf{s}(\mathbf{x}, t)$ from a single time series ε_i is impossible: a wide range of slip patterns could produce the same change in observed strain. Since we have two such series, the inversion remains highly nonunique, but with additional (and reasonable) assumptions we can form some estimate of the possible slip distribution.

The main assumptions are three:

1. We assume that $\mathbf{s}$ is in fact a scalar, with only one nonzero component s: we choose this to be the strike-slip motion.
2. We assume that s is non-negative for all $\mathbf{x}$ and t: that is, that the fault slips only in one direction (in this case right-lateral).
3. We assume that for any value of t, s is nonzero over a region small enough that $\mathbf{G}_i$ is nearly constant over it; in effect, that $s(\mathbf{x}(t), t) = s(t)\delta(\mathbf{x} - \mathbf{x}_s(t))$ so that the integral becomes a multiplication, making (1) into

$$\varepsilon_i(t) = G_i(\mathbf{x}_s(t))s(t) \tag{2}$$

where we have made the location of the slip $\mathbf{x}_s(t)$. This reduction of the integral to a multiplication will also be the case if the area being integrated over is of a fixed size and shape, though in that case the slip becomes the average slip over the area.

Since there is no zero level in the observed strain, it is best to work with the time derivative of the signal; we assume that the change in $\mathbf{x}_s$ is slow enough that we need not include it explicitly, in which case (2) becomes

$$\dot{\varepsilon}_i(t) = G_i(\mathbf{x}_s(t))\dot{s}(t) \tag{3}$$

We now rearrange both the observational and theoretical quantities to give an expression in which the slip amount is decoupled from the Green functions. Define two n-vectors $\mathbf{g}$ and $\mathbf{e}$, with the i-th component of each one being $g_i = G_i$ and $e_i = \dot{\varepsilon}_i$, and define the unit vectors $\mathbf{n}_g = \mathbf{g}/|\mathbf{g}|$ and $\mathbf{n}_e = \mathbf{e}/|\mathbf{e}|$. Then equation (3), applied to all the observations, becomes

$$\mathbf{e}(t) = \mathbf{n}_g(\mathbf{x}(t))\dot{s}(t) \tag{4}$$

The direction of $\mathbf{n}_g$ depends on the ratios of the Green functions $\mathbf{G}_i$, which are a function only of position on the fault.

The method of analysis is thus to find $\mathbf{n}_e(t)$ from the data, perhaps with errors; this will give an acceptable region on the n-dimensional hypersphere. We can then map this region into a region on the fault (usually several regions); the slip must occur in such a region. For a particular location, and direction of $\mathbf{n}_e$, we can solve for the slip as

$$s = |\mathbf{e}|/|\mathbf{g}| \tag{5}$$

For the strain data at Durmid Hill, we have only two observation types; we say that $e_1 = \dot{\varepsilon}_{\mathrm{EW}}$ and $e_2 = \dot{\varepsilon}_{\mathrm{NS}}$, so that $\mathbf{e}$ and $\mathbf{g}$ are 2-dimensional vectors. We can then represent the directions of the unit vectors $\mathbf{n}_g$ and $\mathbf{n}_e$ by a scalar quanitity, namely an angle θ, measured counterclockwise from the 1-axis; a distance measure between two unit vectors is the cosine of the angle between them. We use θ_e for θ inferred from the data, and θ_g for θ computed for different locations on the fault.

This representation suggests a method of displaying all values of $\theta_g(\mathbf{x})$: associating each value of θ with a color hue (in the hue-saturation-brightness description of colors) since these, like θ, lie on a circle. A location with positive EW strain and no NS strain corresponds to $\theta_g = 0$ (red); a location with zero EW strain and positive NS strain corresponds to $\theta_g = \pi/2$ (greenish-yellow); a location with negative EW strain and zero NS strain corresponds to $\theta_g = \pi$ (light blue) and a location with zero EW strain and negative NS strain corresponds to $\theta_g = 3\pi/2$ (blue changing to purple).

Figure 6 shows this representation of $\theta_g(\mathbf{x})$ for these two observables, plotted on the plane of the southern San Andreas fault, adjacent to the DHL strainmeters; more precisely, on a vertical plane along the line shown in the right-hand panel of **Figure 1**, and using the x-coordinates shown on that map. The responses were computed from the Okada (1985) formulas for an elastic halfspace, assuming uniform slip of 1 cm over a square 100 m on a side: a moment of 3×10^{12}N-m, with an equivalent moment magnitude of 2.3 – though this moment assumes what is probably too high a shear modulus for the shallower material at DHL. The color bar below the plot shows how different colors correspond to different normalized responses, which are just the sine and cosine of θ_g. The contour plot below the color bar shows the value of $|\mathbf{g}|$: the units are femtostrain for the assumed source.

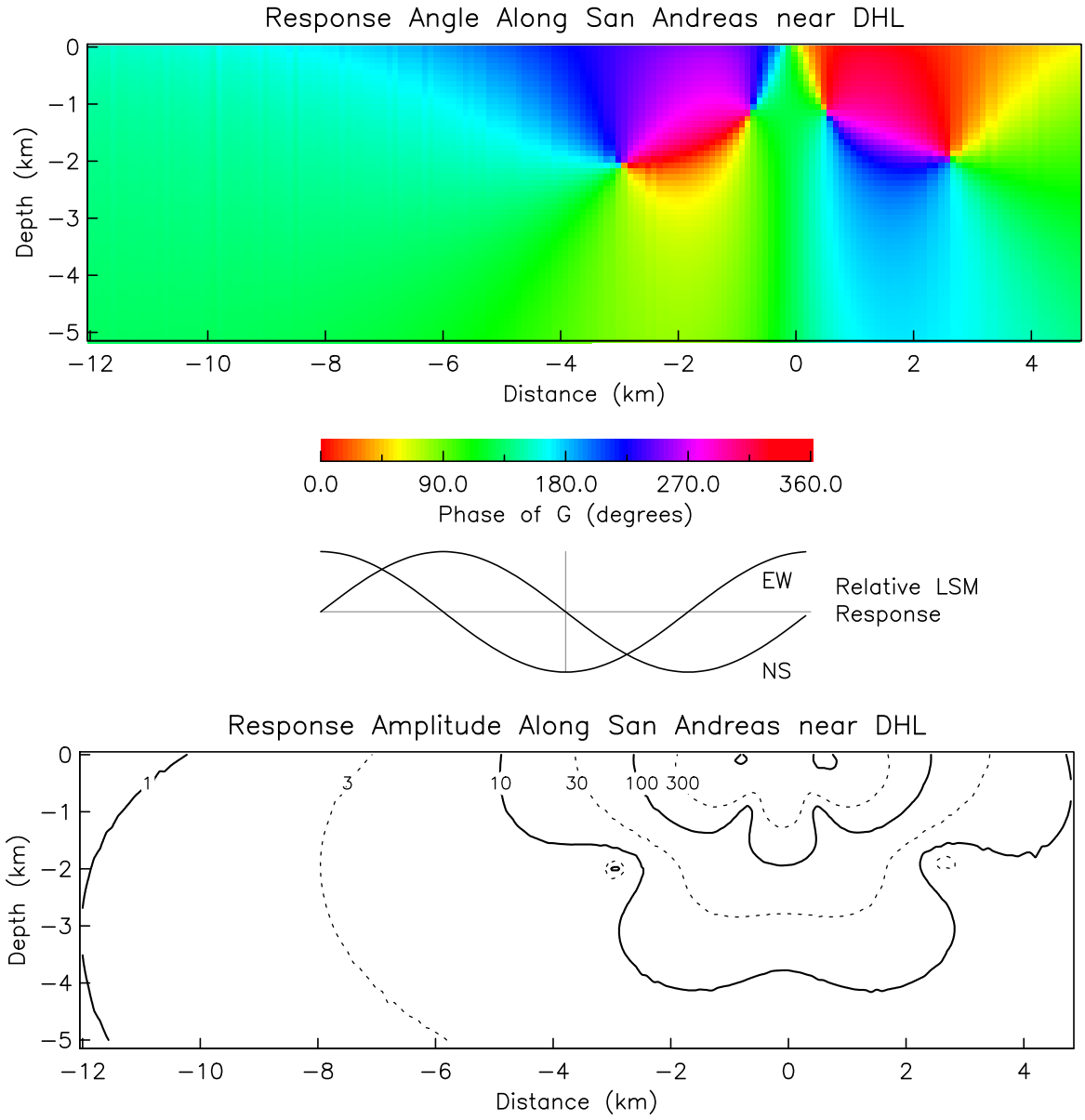

Figure 6

To find the values of $\theta_e(t)$ from the data, we first differentiate the raw 1-Hz data with a FIR filter designed to be a differentiator and lowpass combined (Kaiser and Reed 1977); a cutoff frequency of 0.08 Hz (period 12.5 s), with a 0.015 Hz transition band and 40 dB minimum rejection in the stopband removes fluctuations from microseisms. We then combine the two strain-rate series to find the direction $\theta_e(t)$ and amplitude $|\mathbf{e}(t)$. The error in $\dot{\varepsilon}$ for each component is estimated from the RMS of it just before the start of each strain event. For values of $|\mathbf{e}|$ much larger than the errors, we can approximate the error in θ_e by $\text{atan}(\sigma/|\mathbf{e}|)$ where σ is the error; for values of $|\mathbf{e}|$ closer to σ the pdf of θ_e is non-normal. As a first approximation we make the error in θ_e "infinite" (that is, assume the pdf of θ_e to be uniform over the whole interval $[0, 2\pi)$) for $|be| < 1.5\sigma$. **Figure 7** shows the strains, strain-rates, θ_e, and $|be|$ as a function of time for two of the strain events from **Figure 4**. In the bottom plot we have used a lighter color for θ_e when the amplitude of the strain-rate is less than $0.6 \times 10^{-9}\text{s}^{-1}$, since in that case the errors are very large and the value of θ_e oscillates wildly.

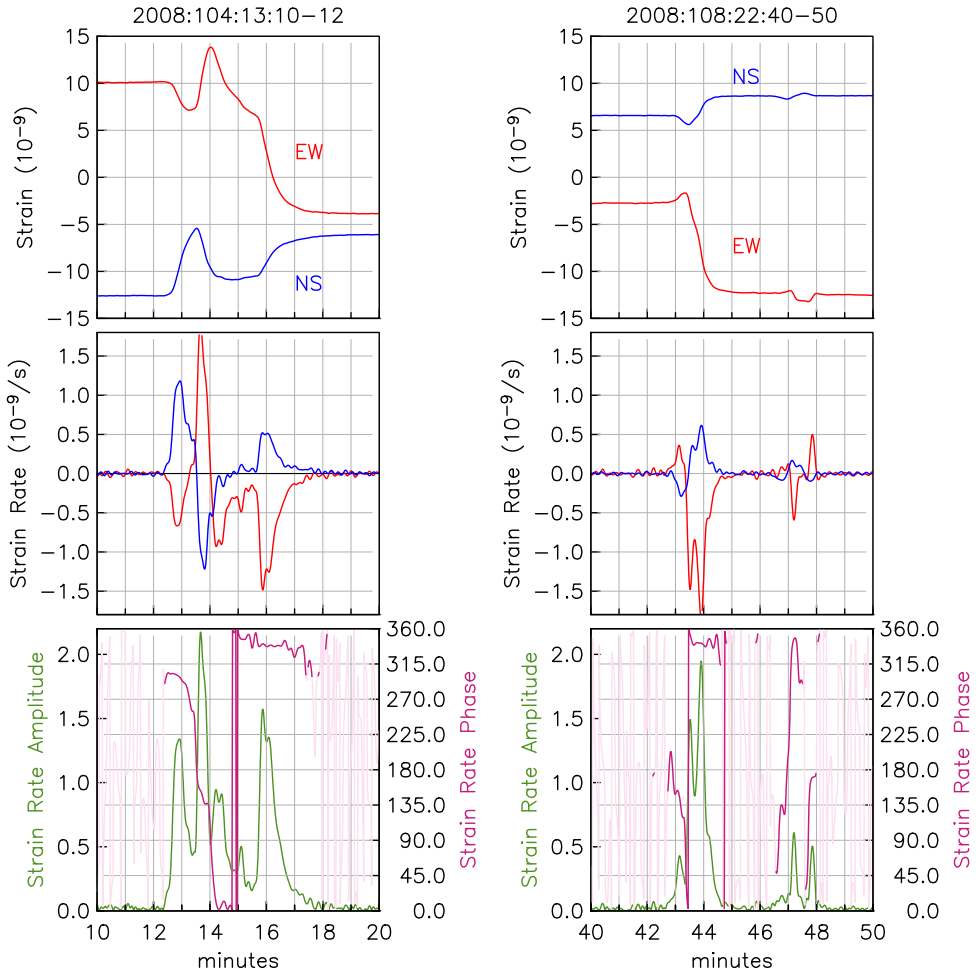

Figure 7

A given range of θ_e will correspond to a possible range for θ_g, which in turn will correspond to areas of the fault plane. If $\theta_e(t)$ is constant, these areas will be fixed, and the most we can do in an inversion is, for each of them, determine the corresponding time history, $s(t)$, of the slip. If θ_e varies with time, so will the corresponding areas on the fault plane. It is a reasonable assumption that the slip at any time is spatially contiguous to where it was at the time just previous: this implies that we should prefer locations for which the areas determined by $\theta_e(t)$ do not jump over intervening ones, and probably, move as little as possible,

For the event on 2008:104:13, we see that there are four subevents, each lasting less than a minute. The first one has a phase angle around 300° and the second (the largest of this sequence) of about 150°. The phase angle then decreases to zero and wraps around, with the last part of the sequence having an angle of 330°: essentially the same for most of the event on 2008:108:22.

How might we interpret this in terms of **Figure 6**? **Figure 8** shows regions that correspond to different phase angles: red for $290° \le \theta_g \le 310°$, green for $140° \le \theta_g \le 160°$, and blue for $320° \le \theta_g \le 340°$. The first and third of these are relatively localized, and interestingly do not reach the surface. There are four locations where these regions touch; as the bottom panel in **Figure 6** shows, the lower two of these correspond to nulls in the amplitude response. So it appears that the slip, if actually concentrated in one

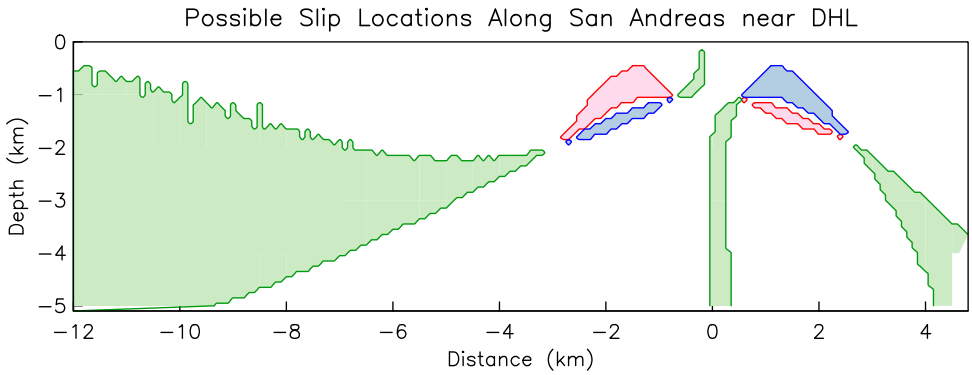

Figure 8

location, must have been close to the strainmeters, and at a depth of about 1 km. **Figure 6** shows that the response in these regions is about 0.1 nε for the specified slip. For the first event on day 104, the cumulative slip (the square root of the sum of the squares of the two offsets) is about 2.2×10^{-8}, which implies a slip over 200 times as large as the slip amount assumed in the bottom panel of **Figure 6**, giving a moment 1.5 magnitude units higher, or 3.9. While this does not correspond to a very large event, it does again demonstrate how sensitive the laser strainmeter data are.

The quality of the inversions above depends in part on the reliability of the Green functions—and this poses something of a challenge. One puzzle we have long been troubled by is that surface loading within a few km of the strainmeters—whether by passing trains or by the seiching of the Salton Sea—causes strains that have the opposite sign from those expected for a uniform halfspace. This is a fairly fundamental departure from a simple model, and needs to be cleared up before doing any inversion for fault slip. Fortunately, the necessary code for loading of a layered halfspace has been developed by Pan *et al.* (2007), and it appears that a suitable shallow structure, with a soft layer overlying a stiff one, can cause the behavior we see (M. Bevis, pers. commun., 2008). In the future we plan to find a Green function for such structure using the program of Wang *et al.* (2003); this should provide much more reliable constraints on the amount and location of slip. Given the (probably) much lower shear modulus of the near-surface material, it may also allow the widespread shallow slip that is suggested by the occurrence of creep observed well to the NW of the two strainmeters (at about the -10 km point in **Figure 6**.)

4. Creep-Related Signals from the El-Mayor/Cucupah Earthquake

The El-Mayor/Cucapah (hereafter EMC) earthquake is named for the two mountain ranges it occurred in; these divide the Mexicali Valley from a another large area below sea level to the west, Laguna Salada. The main plate boundary runs along the Cerro Prieto and Imperial faults in the Mexicali and Imperial valleys, but some slip is transferred to the west, and the faults along the west side of the mountain ranges are assumed to connect to the Elsinore fault to the northwest. A relatively fresh scarp found by Mueller and Rockwell (1995) along the western side of the mountains, called the Laguna Salada fault, is generally assumed to be associated with a large earthquake (magnitude 7.2) in February 1892; the intensity reports are at least consistent with such a location (Hough and Elliot 2004). Just over 118 years later, the EMC earthquake (magnitude 7.2) was also caused by rupture of a fault in the mountains, though the surface rupture is separate from the one that has been associated with the 1892 shock. The mainshock was a somewhat complex event, with an initial rupture around the epicenter (in the Sierra El Mayor) followed about 15 s later by slip running NW along the west edge of the Sierra Cucapah about to its northern end, and the US border, and also running SE of the epicenter.

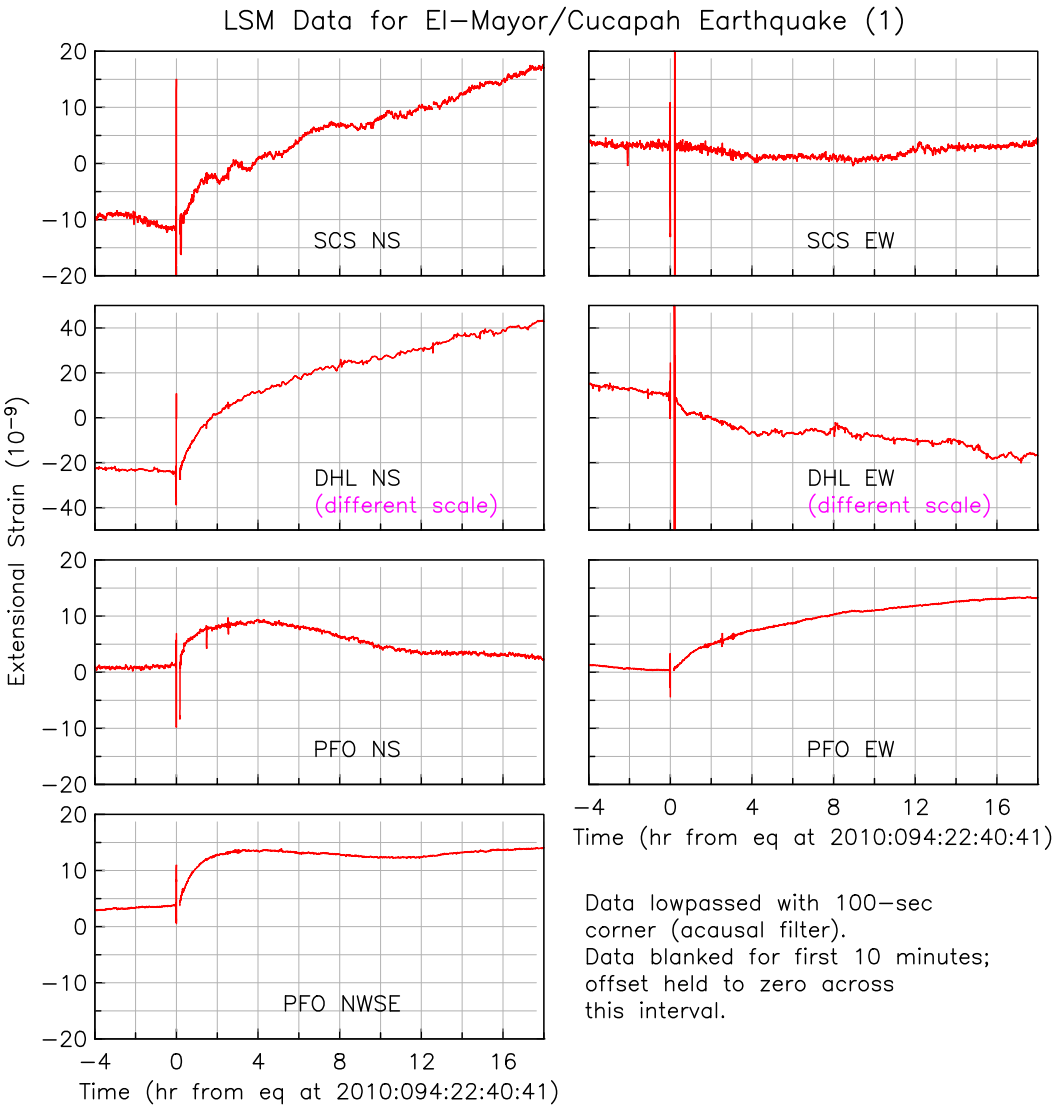

Figure 9

Figure 9 and **Figure 10** show the time series from the seven laser strainmeters installed around the Salton Trough: three at PFO, and two each at SCS and DHL.[2] The data in **Figure 10** run to the end of day 123 (May 4), 30 days after the earthquake.

Figure 9 shows the time immediately before and after the event. All the strainmeters recorded without interruption during the mainshock; but the records cannot be used to find the coseismic offset because of the equivalent of a GPS ‘‘cycle slip’’. The strains from the largest seismic waves are large enough that the laser beam is no longer pointed accurately at the far end; when this happens the interference pattern disappears and strain is not measured. Also, the fringe-detection electronics takes a few minutes to recover. We have about a 5 to 10 minute interval during which we do not have a reliable measure of strain; in the plots we have set the offset to be zero across this gap so that we can best show other changes. Since much more information on coseismic behavior is available from seismic, GPS, and

[2] The instruments at DHL are actually oriented 5° counterclockwise from the cardinal directions, but for simplicity we refer to them as NS and EW.

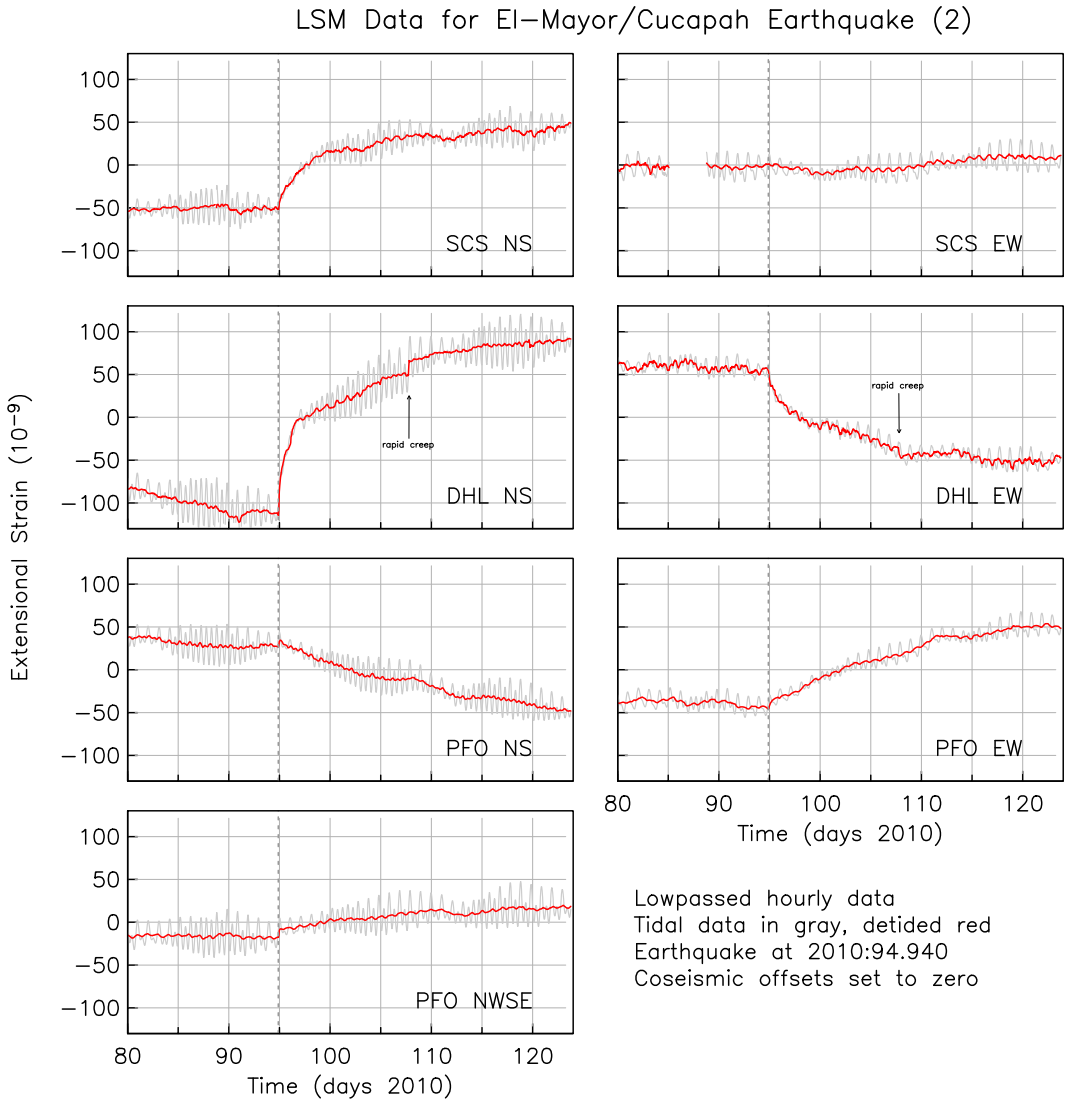

Figure 10

InSAR, the loss of this information while unfortunate, has little impact on understanding the rupture process.[3]

After this interruption the strainmeters give a continuous record of even small deformations. The plot shows the result of lowpassing the original 1-Hz data (filter corner at 100 s) to remove the seismic coda. When this is done these records show immediate, relatively smooth, strain changes at rates much higher than are observed at any other time.

The data in **Figure 9** and **Figure 10** suggest, however, a more complex picture than simple afterslip on the fault that caused the EMC earthquake. Table 1 gives the predicted coseismic strains, and some ratios between them, for the simple uniform-slip model mentioned in the previous section. For the strains at SCS (**Figure 1**) these ratios are in reasonable agreement with what is observed. In particular, the model predicts that the ratio between EW and NS strains is small, something that the data also demonstrate, as

[3] We do have reliable estimates of coseismic offsets from the EW longbase tiltmeter at PFO, and from the more distant strainmeters in Los Angeles and Cholame.

the signal on the EW strain data is very small. A more detailed examination of the EW/NS ratio as a function of position along the rupture plane shows that the smaller values of this ratio occur farther south on the fault, which would imply that the afterslip may be more in the region of the epicenter than at the northern termination of the rupture. As usual, the postseismic deformations are much too large to be caused by the observed aftershocks.

Table 1: Model Coseismic Strains

Model Coseismic Strains	NS	EW	NW	EW/NS	NW/NS
SCS	314	46.4	—	0.15	—
DHL	355	–40.8	—	–0.12	—
PFO	9.4	31.0	55.7	3.3	5.9

We therefore assume, as a first approximation, that the SCS NS data in **Figure 9** and **Figure 10** represent the time history of afterslip on the fault that caused the mainshock. If that were the only process at work, we would expect all the other strainmeter records to look like scaled versions of this time series; that these records do not look like this suggests other sources of strain were triggered by the mainshock.

Looking first at the DHL data, we see a much larger and faster response on the NS, even though the model predicts similar responses for the SCS and DHL NS strains. The ratio of EW to NS response is also much larger than predicted by the model. And, we observe several small steps in these series that are not seen elsewhere (one large event is identified in the figure). Our explanation for all this is that the instruments are recording, not just strains from the EMC earthquake, but also signals from aseismic slip induced on the San Andreas fault, which is only 1.5 km away at the closest.

The idea that the signals at DHL are caused by near-surface slip on the San Andreas fault is also supported by results from Prof. Bilham's creepmeter array; the instrument at Salt Creek, 9 km NW of DHL, showed a few mm of creep coincident with the EMC earthquake. Triggered surface creep from the EMC earthquake was also observed on InSAR data and in the field in the Mecca Hills region, about 30 km NW of DHL (Wei *et al.* 2011)

References

C. R. Allen, M. Wyss, J. N. Brune, A. Grantz, and R. E. Wallace, "Displacement on the Imperial, Superstition Hills, and San Andreas faults triggered by the Borrego Mountain earthquake, in The Borrego Mountain Earthquake of April 9, 1968," *U. S. Geol. Surv. Prof. Pap.,* 787, pp. 87-104 (1972).

K. F. Evans, R. O. Burford, and G. C. P. King, "Propagating episodic creep and the asismic slip behavior of the Calaveras Fault north of Hollister, California," *J. Geophys. Res.,* 86, pp. 3721-3735 (1981).

M. T. Gladwin, R. L. Gwyther, R. H. G. Hart, and K. S. Breckenridge, "Measurements of the strain field associated with episodic creep events on the San Andreas fault at San Juan Bautista, California," *J. Geophys. Res.,* 99, pp. 4559-4565 (1994).

N. Goulty and R. Gilman, "Repeated creep events on the San Andreas Fault near Parkfield, California, recorded by a strainmeter array," *J. Geophys. Res.,* 83, pp. 5415-5419 (1978).

S. E. Hough and A. Elliot, "Revisiting the 23 February 1892 Laguna Salada earthquake," *Bull. Seism. Soc. Am.,* 94, pp. 1571-1578 (2004).

J. F. Kaiser and W. A. Reed, "Data smoothing using low-pass digital filters," *Rev. Sci. Instrum.,* 48, pp. 1447-1454 (1977).

G. C. P. King, R. G. Bilham, J. W. Campbell, and D. P. McKenzie, "Detection of elastic strainfields caused by fault creep events in Iran," *Nature,* 253, pp. 420-423 (1975).

A. T. Linde, M. T. Gladwin, M. J. S. Johnston, and R. L. Gwyther, “A slow earthquake sequence on the San Andreas fault,” *Nature,* 383, pp. 65-68 (1996).

J. Louie, C. R. Allen, D. C. Johnson, S. N. Cohen, and P. C. Haase, “Fault slip in Southern California,” *Bull. Seismol. Soc. Amer.,* 75, pp. 811-833 (1985).

S. Lyons and D. Sandwell, “Fault creep along the southern San Andreas from interferometric synthetic aperture radar, permanent scatterers, and stacking,” *J. Geophys. Res.,* 108, pp. ETG 11-1-ETG 11-24 (2003).

K. J. Mueller and T. F. Rockwell, “Late Quaternary activity of the Laguna Salada fault in northern Baja California, Mexico,” *Geol. Soc. Amer. Bull.,* 107, pp. 8-18 (1995).

E. Pan, M. Bevis, F. Han, H. Zhou, and R. Zhu, “Surface deformation due to loading of a layered elastic half-space: a rapid numerical kernel based on a circular loading element,” *Geophys. J. Int.,* 171, pp. 11-24 (2007).

M. J. Rymer, “Triggered surface slips in the Coachella Valley area associated with the 1992 Joshua Tree and Landers, California, earthquakes,” *Bull. Seismol. Soc. Amer.,* 90, pp. 832-848 (2000).

M. J. Rymer, J. Boatwright, L. C. Seekins, J. D. Yule, and J. Liu, “Triggered surface slips in the Salton Trough associated with the 1999 Hector Mine, California, earthquake,” *Bull. Seismol. Soc. Amer.,* 92, pp. 1300-1317 (2002).

J. C. Savage, M. Lisowski, N. E. King, and W. K. Gross, “Strain accumulation along the Laguna Salada fault, Baja California, Mexico,” *J. Geophys. Res.,* 99, pp. 18109-18116 (1994).

R. V. Sharp, K. E. Budding, J. Boatwright, M. J. Ader, M. G. Bonilla, M. M. Clark, T. E. Fumal, K. K. Harms, J. J. Lienkaemper, D. M. Morton, B. J. O’Neill, C. L. Ostergren, D. J. Ponti, M. J. Rymer, J. L. Saxton, and J. D. Sims, *Surface faulting along the Superstition Hills fault zone and nearby faults associated with the earthquakes of 24 November 1987,* 79, pp. 252-281 (1989).

K. E. Sieh and P. L. Williams, “Behavior of the southernmost San Andreas fault during the past 300 years,” *J. Geophys. Res.,* 95, pp. 6629-6645 (1990).

R. Uhrhammer, L. S. Gee, M. Murray, D. Dreger, and B. Romanowicz, “The Mw 5.1 San Bautista, California Earthquake of 12 August 1998,” *Seismol. Res. Lett.,* 70, pp. 10-18 (1999).

R. Wang, F. L. Martin, and F. Roth, “Computation of deformation induced by earthquakes in a multi-layered elastic crust: FORTRAN programs EDGRN/EDCMP,” *Comput. Geosci.,* 29, pp. 195-207 (2003).

M. Wei, D. Sandwell, Y. Fialko, and R. Bilham, “Slip on faults in the Imperial Valley triggered by the 4 April 2010 Mw 7.2 El Mayor/Cucapah earthquake revealed by InSAR,” *Geophys. Res. Lett.,* 38, p. L01308 (2011).

R. L. Wesson, “Dynamics of fault creep,” *J. Geophys. Res.,* 93, pp. 8929-8951 (1988).

P. L. Williams, S. F. McGill, K. E. Sieh, C. R. Allen, and J. N. Louie, “Triggered slip along the San Andreas fault after the 8 July 1986 North Palm Springs earthquake,” *Bull. Seismol. Soc. Amer.,* 78, pp. 1112-1122 (1988).